

Purdue University

Purdue e-Pubs

---

International Refrigeration and Air Conditioning  
Conference

School of Mechanical Engineering

---

2022

## Enhancement of the Critical Heat Flux During the Cooling of Power Electronics – Part 2

Stefan Wettengel

Oliver Ziegler

Andreas Kluge

Lars Lindenmüller

Steffen Bernet

*See next page for additional authors*

Follow this and additional works at: <https://docs.lib.purdue.edu/iracc>

---

Wettengel, Stefan; Ziegler, Oliver; Kluge, Andreas; Lindenmüller, Lars; Bernet, Steffen; and Fischer, Gerd, "Enhancement of the Critical Heat Flux During the Cooling of Power Electronics – Part 2" (2022). *International Refrigeration and Air Conditioning Conference*. Paper 2287. <https://docs.lib.purdue.edu/iracc/2287>

This document has been made available through Purdue e-Pubs, a service of the Purdue University Libraries. Please contact [epubs@purdue.edu](mailto:epubs@purdue.edu) for additional information. Complete proceedings may be acquired in print and on CD-ROM directly from the Ray W. Herrick Laboratories at <https://engineering.purdue.edu/Herrick/Events/orderlit.html>

---

**Authors**

Stefan Wettengel, Oliver Ziegler, Andreas Kluge, Lars Lindenmüller, Steffen Bernet, and Gerd Fischer

## Enhancement of the Critical Heat Flux During the Cooling of Power Electronics – Part 2

Stefan WETTENGEL<sup>1\*</sup>, Oliver ZIEGLER<sup>2</sup>, Andreas KLUGE<sup>3</sup>,  
Lars LINDENMÜLLER<sup>1</sup>, Steffen BERNET<sup>1</sup>, Gerd FISCHER<sup>3</sup>

<sup>1</sup>Chair of Power Electronics, Technische Universität Dresden,  
Dresden, Saxony, Germany  
[stefan.wettengel@tu-dresden.de](mailto:stefan.wettengel@tu-dresden.de)

<sup>2</sup>Bitzer-Chair of Refrigeration, Cryogenics and Compressor  
Technology, Technische Universität Dresden  
Dresden, Saxony, Germany  
[oliver.ziegler@tu-dresden.de](mailto:oliver.ziegler@tu-dresden.de)

<sup>3</sup>F&S PROZESSAUTOMATION GmbH,  
Dohna (Dresden), Saxony, Germany  
[gerd.fischer@fs-aut.de](mailto:gerd.fischer@fs-aut.de)

\* Corresponding Author

### ABSTRACT

In a previous paper the authors had presented a novel, electrically insulating heatsink concept for power semiconductor switches (IGBT) based on natural circulation (Hu, et al., 2021). The working principle of the heatsink relies on pool boiling on the bottom of a vapor chamber and film condensation on the condenser above. An insulating refrigerant is used. The principle of this heatsink is introduced in a patent by Fischer, Langebach and Lindenmüller (Germany, Patent No. DE102017215952B3, 2017). In the mentioned paper (Hu, et al., 2021) the authors compared the direct contact between the IGBT's bottom plate and the refrigerant with the utilization of a copper interface plate with a defined surface structure with open microgrooves. Other methods for increasing the critical heat flux (CHF) in the chamber, such as silicon pin-fins or free copper particles, were discussed as well.

In this paper the authors present an extension to the research done before. Since the direct contact between the power semiconductor module and the refrigerant has shown crucial drawbacks in CHF and thus overall cooling performance, this work focusses on the use of metal interface plates between the IGBT and the refrigerant. The influence of material choice and surface texture are discussed and experimentally verified. Additionally, a comparison between two different refrigerants and their effect on cooling performance and CHF is shown. As a conclusion the use of sandblasted interface plates is recommended. Copper should be used, aluminum can be used, but with lower thermal performance.

### 1. INTRODUCTION

Key challenges in modern power electronics include miniaturization and thus a rising power density. Since any electrical or electronic system causes losses – including semiconductor switches – active cooling is often inevitable. Especially in applications with high power and high power density, water cooling can be a favorable solution. Today, power electronics are in use from low to high voltage applications. Medium voltage applications include medium voltage direct current (MVDC), for example as a MVDC grid (Siemens Energy, 2021) or for power distribution on ships, see e.g. (IEEE Standards Association, 2018). Further applications are for example medium voltage motors, e.g.

for pumps, compressors and fans (Siemens AG, 2021) or the link of renewables directly to the medium voltage grid, see e.g. (Islam, Mahfuz-Ur-Rahman, Muttaqi, & Sutanto, 2019).

The combination of medium voltage and water cooling, however, can be challenging. One of the challenges is the avoidance of leakage current through the coolant, caused by different heatsink potentials. An insulated heatsink could provide a significant advantage in such applications – especially, if extensive coolant de-ionization can be avoided.

The most important semiconductor switch in modern power electronics is the Insulated-Gate Bipolar Transistor (IGBT). IGBTs are available from small, low-power packages to high-power modules with permissible voltages in the range of up to several kilovolts and currents in the range of up to multiple kiloamperes. The IGBT module used in this work is the *FZ1200R45KL3\_B5* with a maximum voltage of 4.5 kV and a maximum average current of 1.2 kA, see (Infineon Technologies AG, 2018).

In a previous paper (Hu, et al., 2021) the authors presented an insulating heatsink based on pool boiling of an insulating refrigerant. However, a direct contact between the IGBT's bottom plate and the coolant did not lead to satisfying results. The use of a metal interface plate, on the other hand, was determined to be a promising approach. This paper extends the analysis for different interface plates. In addition, another condenser is used to avoid a potential bottleneck suggested by past experiments.

## 2. EXPERIMENTAL SETUP AND REFRIGERANTS

### 2.1. Test Setup

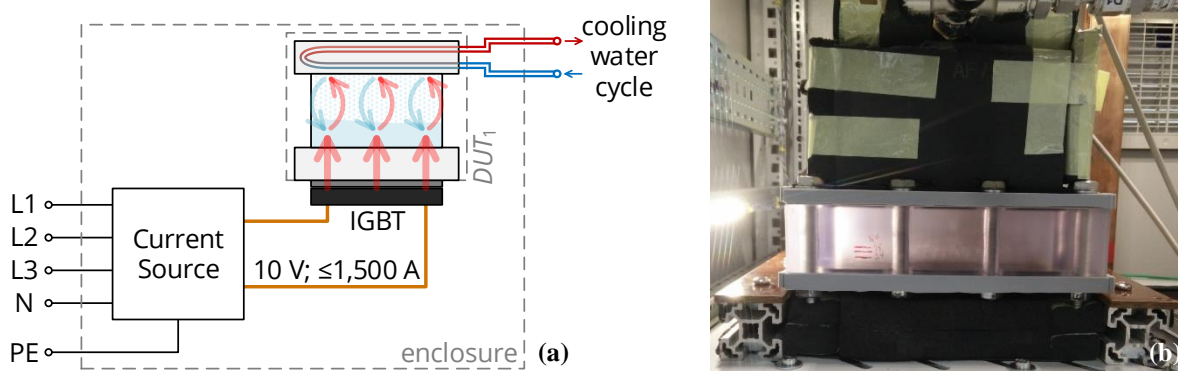


**Figure 1:** (a) Basic principle of the test setup. (b) Photograph of the boiling cooler inside the enclosure

The test setup is shown in Figure 1 both as a simplified sketch (a) as well as a photograph of the device under test inside an electrical cabinet (b). The device under test (DUT) consists of a metal cover containing a heat exchanger (condenser) on top, a polycarbonate frame as an insulating spacer in the middle section<sup>1</sup> and a metal interface plate on the bottom. The interface plate acts as an evaporation/boiling surface on the inside of the vapor chamber and is also the mounting plate for the IGBT on the outside on the bottom of the heat sink. A 1.2 kA IGBT is used as a heat source. This results in a more realistic heat transfer into the interface plate (and thus the heatsink) than with e.g. a purely resistive heat source emulating a power semiconductor. The test setup used in this work is fundamentally the same as in a previous publication – this includes the uncertainty of measured and calculated parameters, see (Hu, et al., 2021). The locations of heat and pressure sensors inside the DUT are shown in a cut view of the cooler shown in Figure 2.

<sup>1</sup> It should be noted that the heatsink used in this work does currently not provide electrical insulation, since metal bolts are used for assembly, as seen in Figure 1 (b).

All other parameter used for the evaluation of the DUT's cooling performance are calculated from the measured values linked to the sensors shown in Figure 2.

In the previous paper (Hu, et al., 2021) the IGBT base plate temperatures were measured at two points inside the IGBT module through small, drilled holes in the top side of the module's enclosure. The internal sensors are surrounded by silicone, which leads to a slow thermal response and a bad thermal contact in some cases. Since the exact sensor locations are not visible from the outside, this is often only noticeable after an experiment has been performed. In this paper they are not used for thermal calculations. Instead a thermocouple placed on the IGBT's base plate, directly underneath one of the semiconductor chips (which are located on the inner side of the base plate) is used to determine base plate temperature  $T_{BP}$ . The condenser is supplied with cooling water with a constant inlet temperature of  $T_F = 40\text{ }^\circ\text{C}$  and a constant volume flow of  $\dot{V}_W \approx 10\text{ l/min}$ .

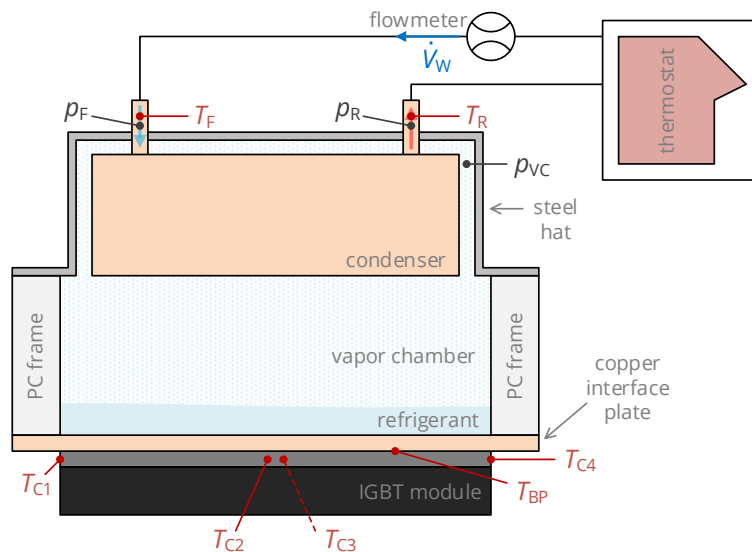


**Figure 2:** Sensor locations in and on the device under test. Measured parameters are IGBT case temperatures  $T_{C1} \dots T_{C4}$ , IGBT base-plate temperature  $T_{BP}$ , flow and return flow temperatures  $T_F$  and  $T_R$  and pressures  $p_F$  and  $p_R$ , vapor chamber pressure  $p_{VC}$  and water flow rate  $\dot{V}_W$

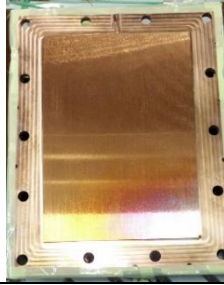


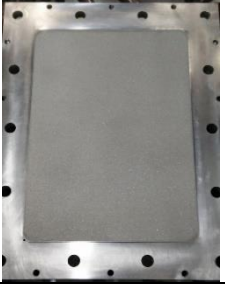
For heat flux estimations the area of heat flow into the liquid refrigerant has to be known. Different surface features and finishes strongly influence the actual surface area. It was already shown in the paper by (Hu, et al., 2021) that different surface conditions led to different heat fluxes. However for a practical application the cross-sectional area  $A_0$  of the refrigerant pool, which indicates the heat transfer area for evaporation, is the most relevant parameter. It depends on the distances of the PC frame's inner walls and is calculated as  $A_0 = 185\text{ mm} \cdot 150\text{ mm} = 27,750\text{ mm}^2$ .

## 2.2. Interface Plates

In the following discussion four different interface plates are used and their impact on thermal performance is analyzed. Interface plates A, B and C are made from copper and have different surface features. Interface plate D has the same surface finish as interface plate C but is made from aluminum. The four interface plates are listed in Table 1 together with key properties.

To illustrate the dimensions of the microgrooves in interface plate A, a sketch depicting the side view of the microgrooves can be seen in (Hu, et al., 2021). The distance between the microgrooves corresponds to the capillary length of *Novec-649* at a saturated temperature of  $T_{sat} = 65\text{ }^\circ\text{C}$ . In the case of the sandblasted interface plates the surface roughness could be determined to be  $R_a \approx 8.2\text{ }\mu\text{m}$  and  $R_z \approx 53.9\text{ }\mu\text{m}$  for interface plate C and  $R_a \approx 5.7\text{ }\mu\text{m}$  and  $R_z \approx 36.3\text{ }\mu\text{m}$  for interface plate D respectively.

**Table 1:** List of interface plates used in this work

Name	A	B	C	D
Photograph				
Material	Copper	Copper	Copper	Aluminum
Thickness $d_{IP}$	7 mm + groves	8.5 mm	8.5 mm	8.0 mm
key properties	surface with micro-grooves	smooth surface	sandblasted surface	sandblasted surface

### 2.3. Comparison of Refrigerants

In addition to the analysis of different interface plates, two different refrigerants are used and compared within this paper. Key parameters of the refrigerants *Novec-649* and *Refr. 2* are listed in Table 2. Italic properties of *Refr. 2* are in comparison to *Novec-649*. Thermophysical properties of both refrigerants, especially the dependence of saturation temperature on pressure  $T_{sat} = f(p_{VC})$  inside the vapor chamber, are extracted from REFPROP 10 (Lemmon, Bell, Huber, & McLinden, 2018).

**Table 2:** Comparison of key parameters of the refrigerants used in this paper

Name	density	boiling point	vaporization heat	GWP	ODP	isolation voltage	Source
<i>Novec-649</i>	1,60 g/cm <sup>3</sup>	49,0 °C	88 kJ/kg	1	0	>15 kV/mm	(3M Company, 2009)
<i>Refr. 2</i>	<1,60 g/cm <sup>3</sup>	<49 °C	>88 kJ/kg	2	0	<15 kV/mm	-

## 3. EXPERIMENT

### 3.1. Preparation

Before each experiment the vapor chamber is evacuated using a vacuum pump. The cooler is then filled with one charge to four changes of refrigerant. Each charge is equal to one refrigerant cylinder, completely filled with liquid phase, which holds a volume of 142 ml. This results in a refrigerant weight of 227 g per charge for *Novec-649* and 193 g for *Refr. 2*, respectively. This corresponds to a refrigerant height of  $\approx 4$  mm above the boiling surface, per charge. Next, the thermostat is turned on and the inlet temperature is set to its nominal value. During the experiment IGBT is held in its on-state by applying a positive DC gate-emitter voltage  $V_{GE} > 15$  V.

### 3.2. Procedure

The experiment itself is performed by increasing the IGBT's losses and thereby heat output in steps of 250 W or 500 W until either the IGBT module base plate temperature reaches a critical value (corresponding to the maximum junction temperature inside the IGBT chip) or until CHF is reached. CHF can be detected by a steep increase of base plate temperature  $T_{BP}$  at the same time as a steep decrease in vapor chamber pressure  $p_{VC}$ . In Figure 3 (a) measured

temperatures for base plate  $T_{BP}$ , water flow  $T_F$  and water return flow  $T_R$  are shown together with the temperature  $T_{VC}$  of the vapor chamber, which is calculated from the chamber pressure  $p_{VC}$  shown in Figure 3 (b). The experiment shown in Figure 3 is performed with interface plate C and a filling of two charges of *Novec-649*. CHF can be observed close to the end of the experiment.

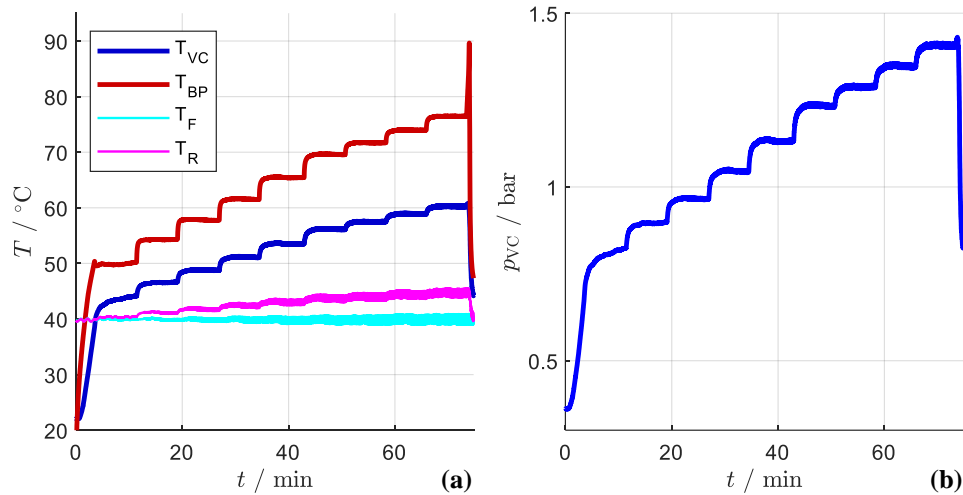


**Figure 3:** (a) Measured temperatures of base plate  $T_{BP}$ , cooling water flow  $T_F$  and return flow  $T_R$ ; calculated temperature of vapor chamber  $T_{VC}$ . (b) Measured vapor chamber pressure  $p_{VC}$ . Experiment with interface plate C and two charges of *Novec-649*

### 3.3. Analysis

In order to analyze the heat sink's performance, additional parameters are calculated from the measured curves using the following equations.

$$\dot{Q}_W = (T_R - T_F) \cdot c_W \cdot \dot{V}_W \cdot \rho_W \quad (1)$$

The heat dissipation  $\dot{Q}_W$  into the cooling water is calculated according to (1) from flow and return flow temperatures  $T_R$  and  $T_F$ ; thermal capacity  $c_W$ , flow rate  $\dot{V}_W$  and density  $\rho_W$  of the cooling water. Flow and return flow temperatures, as well as flow rate are measured during the experiment. The flow rate is approximately constant. The thermal capacity and density of water are known values with  $c_W \approx 4.418$  kJ/(kg·K) and  $\rho_W \approx 1$  g/cm<sup>3</sup>.

$$\dot{q} = \frac{\dot{Q}_W}{A_0} \quad (2)$$

The heat flux  $\dot{q}$  is calculated from the heat dissipation  $\dot{Q}_W$  into the cooling water and the cross-sectional area  $A_0$  of the vapor chamber, see (2).

$$T_S = T_{BP} - \dot{q} \cdot \frac{d_{IP}}{\lambda_{IP}} \quad (3)$$

The direct measurement of the surface temperature of the boiling surface on the bottom of the vapor chamber has proven to be problematic. Glue or tape would cover the sensor and potentially falsify the measured temperatures. On the other hand the sensor could separate itself from the interface plate as well. Both effects have led to problems – therefore the boiling surface temperature  $T_S$  is calculated by (3) from the measured temperature of base plate  $T_{BP}$ , the calculated heat flux  $\dot{q}$  and the thickness  $d_{IP}$  and thermal conductivity  $\lambda_{IP}$  of interface plate itself. The thermal conductivity of copper and aluminum are known values with  $\lambda_{IP} \approx 380$  W/(m·K) for copper and  $\lambda_{IP} \approx 236$  W/(m·K) for aluminum.

To calculate the superheat temperature  $T_S - T_{\text{sat}}$ , the saturation temperature  $T_{\text{sat}}$  is obtained from the pressure  $p_{\text{VC}}$  inside the vapor chamber, see section 2.3.

Figure 4 shows the calculated boiling surface temperature  $T_S$  and the saturation temperature  $T_{\text{sat}}$  of the refrigerant *Refr. 2* as well as the calculated heat flux  $\dot{q}$ . At the end of the experiment a spike in the boiling surface temperature  $T_S$  can be observed. It is not present in  $p_{\text{VC}}$ , see Figure 3 (b), and therefore does not exist in  $T_{\text{sat}}$ . This is a clear indicator of CHF being reached. The experiment has to be stopped within a few seconds in this case, to prevent overheating of (and potential damage to) the IGBT.

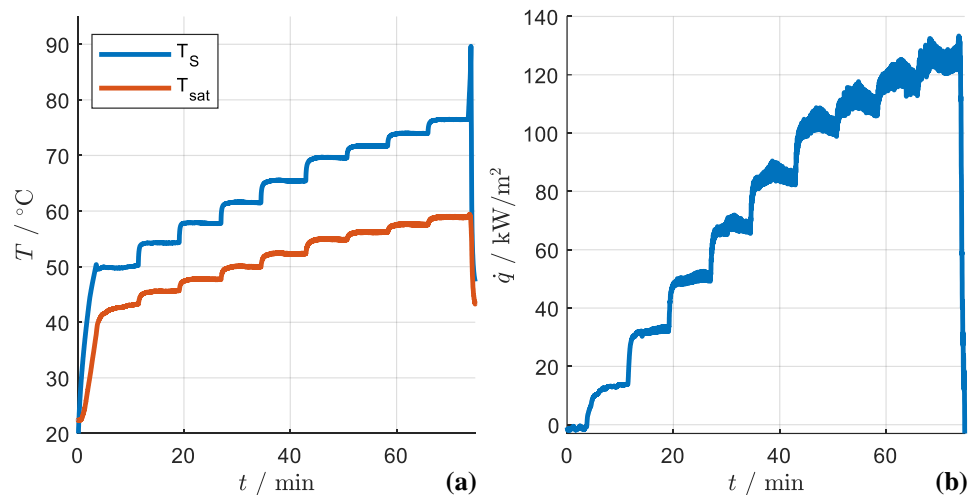


**Figure 4:** (a) Calculated: temperature of boiling surface  $T_S$ , saturation temperature  $T_{\text{sat}}$ . (b) calculated heat flux  $\dot{q}$ . Experiment with interface plate C and two charges of *Novec-649*

Based on the measured curves, parameters are extracted and the heatsink's performance is evaluated. Parameters of interest are the heat flux  $\dot{q}$  for different values for the surface superheat temperature  $T_S - T_{\text{sat}}$  and, for example, the relationship between boiling surface temperature  $T_S$  and heat dissipation  $\dot{Q}_W$ . The resulting dependencies are compared under different conditions in section 4.

## 4. EXPERIMENTAL RESULTS

In a previous publication the condenser has been identified as a potential bottleneck (Hu, et al., 2021), preventing measurements at higher heat flux levels. In this work a new, larger condenser is used. To verify the effects on the heat flux, measurements with two charges of *Novec-649* are compared in Figure 5. As shown, for a surface superheat temperature of  $> 10$  K the new condenser leads to a higher heat flux than the first condenser. It should also be noted that for superheat temperatures of  $T_S - T_{\text{sat}} > 19$  K the cooling water inlet temperature  $T_F$  has to be successively reduced to allow for a higher thermal output without overheating the IGBT; leading to an inlet temperature of  $20$   $^{\circ}\text{C}$  at the final data point ( $23.7$  K,  $122,8$   $\text{kW}/\text{m}^2$ ). For the new condenser a lowering of the inlet temperature to  $T_F = 30$   $^{\circ}\text{C}$  is only necessary for the last three data points, for  $T_S - T_{\text{sat}} > 25$  K. The new condenser therefore allows for experiments with higher thermal output and thus potentially higher heat flux rates.

In Figure 6 the dependency of heat flux on surface superheat temperature is shown for both refrigerants and different refrigerant levels, reaching from one to three charges or  $142$  ml to  $426$  ml of refrigerant, respectively. All measurements are performed using interface plate C. There is only a negligible effect of the refrigerant level on the cooling performance. The effect of refrigerant choice is also small, CHF is reached only when using *Novec-649*, however, CHF could not be reached within the thermal limits of the IGBT using *Refr. 2* as a refrigerant.



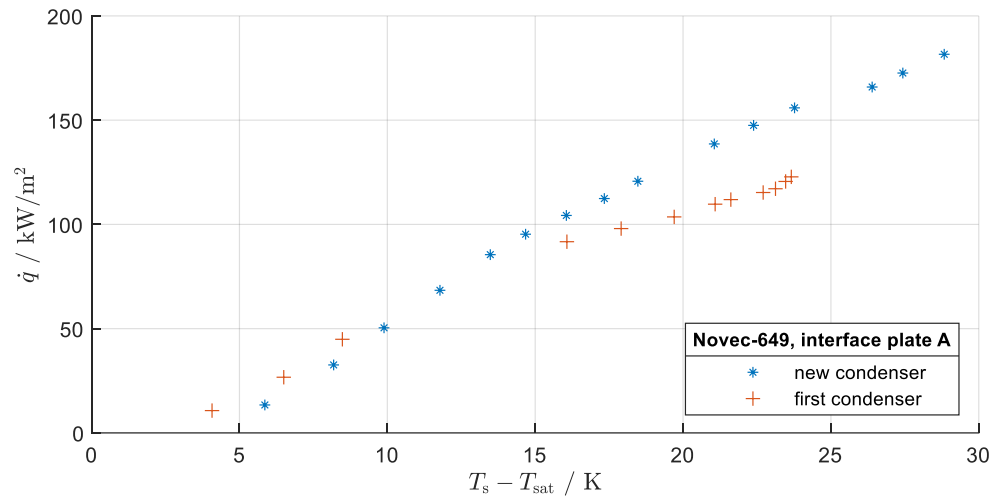


**Figure 5:** Heat flux versus surface superheat temperature. Comparison of first and new condenser. Interface plate A: copper plate with microgrooves, cooler filled with two charges of *Novec-649*

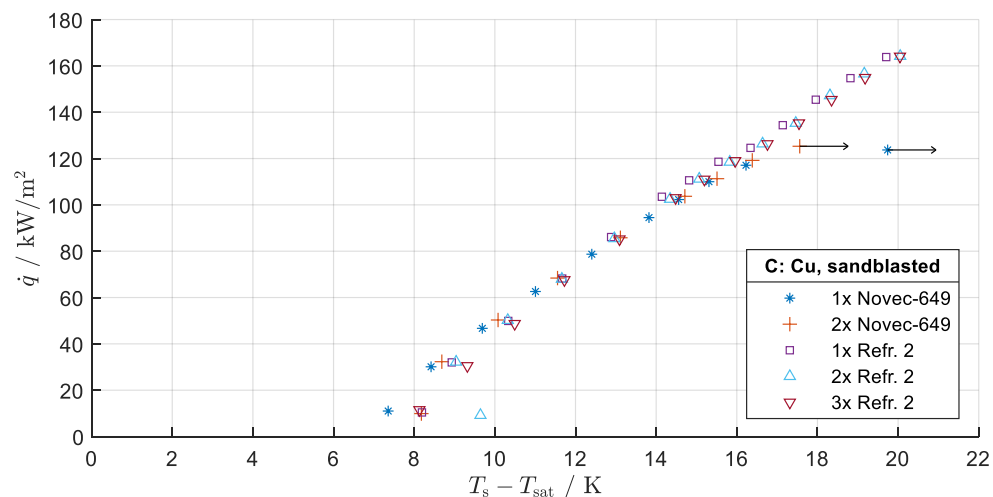


**Figure 6:** Heat flux versus surface superheat temperature. Interface plate C: sandblasted copper plate. Comparison of different number of refrigerant charges of *Novec-649* (227 g per charge) and *Refr. 2* (193 g per charge)

Further experiments are evaluated with two charges of refrigerant. This is seen as a compromise between the use of a low amount of refrigerant (reducing cost and potential environmental impact) and practical considerations – especially a higher tolerance to a not perfectly level positioning of a possible future inverter employing pool boiling heatsinks as described in this paper.

In Figure 7 a comparison of heat flux versus surface superheat temperature is shown for the four different interface plates. In all four experiments *Novec-649* is used. In the experiments with both the sandblasted copper plate and the sandblasted aluminum plate CHF is reached. Below CHF and for  $T_s - T_{sat} > 10$  K, of the four interface plates, the sandblasted copper plate, interface plate C, has the highest heat flux at the same surface superheat temperature. The smooth copper plate and the sandblasted aluminum plate have a similar thermal performance, with the smooth copper plate not reaching CHF. The copper plate with grooves has a thermal performance in between the other interface plates, but does also not reach CHF.

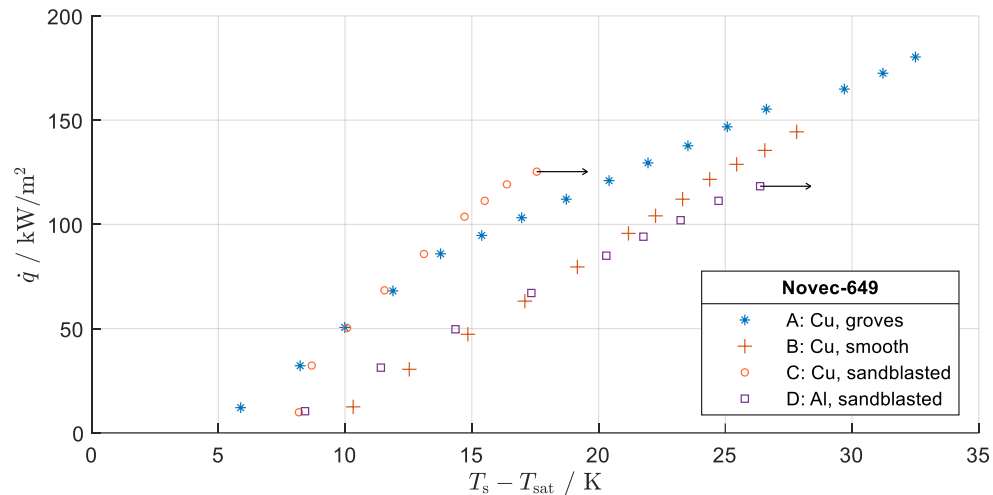


**Figure 7:** Heat flux versus surface superheat temperature. Comparison of different interface plates, cooler filled with two charges of *Novec-649*

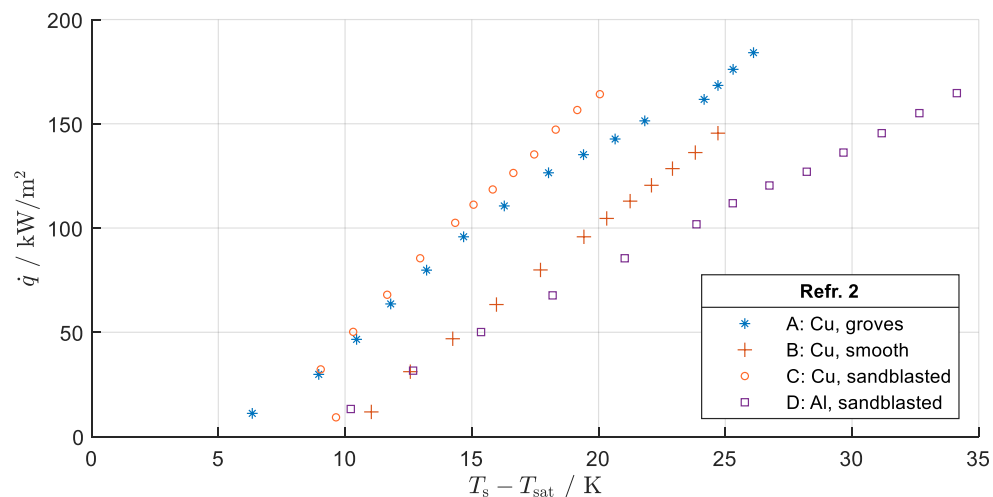


**Figure 8:** Heat flux versus surface superheat temperature. Comparison of different interface plates, cooler filled with two charges of *Refr. 2*

A comparison equivalent to Figure 7, but using two charges of *Refr. 2*, is shown in Figure 8. With the use of *Refr. 2* CHF is not reached, regardless of the interface plate used in the experiment. This allows for an evaluation independently of CHF considerations. Interface plate C, the sandblasted copper plate, is showing the highest heat flux at the same surface superheat temperature for  $T_s - T_{\text{sat}} \geq 9$  K. The interface plates B and D are similar for a low surface superheat temperature of  $T_s - T_{\text{sat}} < 15$  K. At higher temperatures the sandblasted aluminum plate is showing the lowest heat flux. As with *Novec-649*, the copper plate with groves can be observed to be located in between the smooth and the sandblasted copper plate.

In the practical application of cooling power electronic components, the heat sink's surface temperature for a given power output is an important factor. To complete the evaluation of the different interface plates, Figure 9 shows the boiling surface temperature  $T_s$  versus the power dissipation  $\dot{Q}_W$ . For the same heat flow  $\dot{Q}_W$ , a lower temperature  $T_s$  generally results in a lower case temperature  $T_C$  and thus a lower chip temperature inside the IGBT. For both refrigerants the best cooling performance can be observed for both the copper plate with grooves and the sandblasted copper plate. Both perform similarly, however CHF is reached with the sandblasted plate using *Novec-649*. The sandblasted

aluminum plate and the smooth copper plate partially show a similar performance. Over a larger range the smooth copper plate demonstrates a better performance than the aluminum plate, however. As with the sandblasted copper plate, CHF is reached with the sandblasted aluminum plate using *Novec-649*.

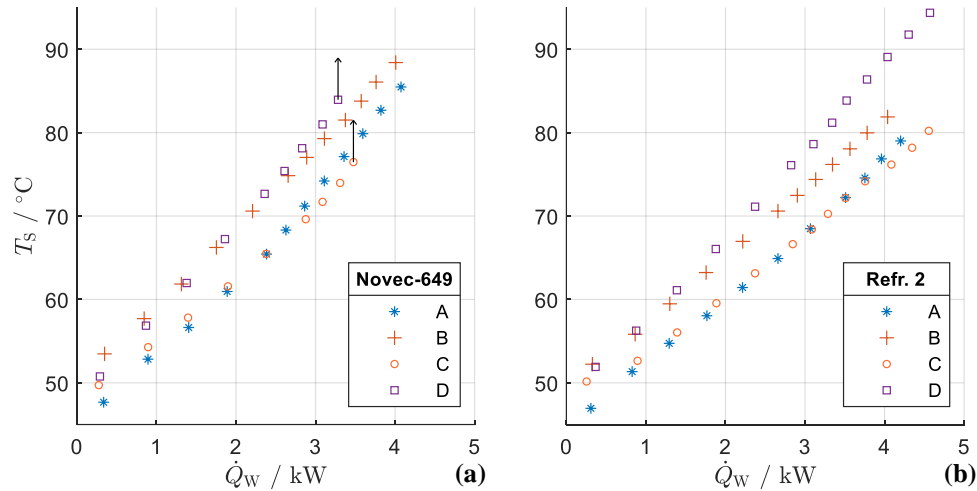


**Figure 9:** Boiling surface temperature versus power dissipated into cooling water. Comparison of different interface plates. Refrigerant volume: two charges, (a) *Novec-649*; (b) *Refr. 2*

## 5. CONCLUSIONS

Even though a metal interface plate between IGBT and refrigerant acts as an additional thermal resistance, the overall thermal performance of the cooler is increased by using an interface plate. If CHF can be avoided in the target application (by reducing heat flux or use of *Refr. 2*), usage of a sandblasted copper plate is generally recommended. Manufacturing effort and cost for the grooved copper plate can be avoided. To accommodate weight and cost constraints, the sandblasted aluminum plate can be a viable alternative – but with lower thermal performance. Smooth plates should be avoided, since they show a lower thermal performance than other solutions using the same material.

Future work will focus more directly on the power electronic modules. Research could potentially aim at junction temperature measurement and the estimation of thermal parameters, e.g. thermal resistance  $R_{thJA}$  and thermal capacitance  $C_{thJA}$  from the semiconductor's junction to the cooling water, as well as the direct comparison of thermal performance to state-of-the-art water cooling heatsinks.

## NOMENCLATURE

$A_0$	boiling area	(mm <sup>2</sup> )
$C_{thJA}$	thermal capacitance: junction-ambient	(J/K)
$c_w$	specific heat capacity, water	(J/(kg·K))
$d_{IP}$	thickness, interface plate	(mm)
$p_F, p_R$	flow and return flow pressure	(bar)
$p_{VC}$	vapor chamber pressure	(bar)
$\dot{q}$	heat flux	(W/mm <sup>2</sup> )
$\dot{Q}_W$	heat dissipation into cooling water	(W)
$R_{thJA}$	thermal resistance: junction-ambient	(K/W)
$T_{BP}$	IGBT base plate temperature	(°C)
$T_{C1} \dots T_{C4}$	measured case temperatures	(°C)

$T_F, T_R$	flow and return flow temperatures	(°C)	
$T_S$	boiling surface temperature	(°C)	
$T_{sat}$	saturated temperature	(°C)	
$V_{GE}$	gate-emitter voltage of the IGBT	(V)	
$\dot{V}_W$	cooling water flow rate	(l/min)	
$\lambda_{IP}$	thermal conductivity, interface plate	(W/(m·K))	
$\rho_w$	density, water	(g/cm <sup>3</sup> )	
A...D	names of the interface plates	IGBT	insulated-gate bipolar transistor
CHF	critical heat flux	MVDC	medium voltage direct current
DUT	device under test	ODP	ozone depletion potential
GWP	global warming potential	PC	polycarbonate
HTC	heat transfer coefficient	Refr. 2	Refrigerant 2

## REFERENCES

- 3M Company. (2009). *Product Information : 3M Novec 649 Engineered Fluid*. St. Paul, MN. (datasheet).
- Fischer, G., Langebach, R., & Lindenmüller, L. (2017). *Germany. Patent No. DE102017215952B3*. Retrieved from <https://depatisnet.dpma.de/DepatisNet/depatisnet?window=1&space=menu&content=treffer&action=bibdat&docid=DE102017215952B3>
- Hu, Y., Ziegler, O., Thomas, C., Hesse, U., Wettengel, S., Kluge, A., . . . Fischer, G. (2021). Enhancement of the Critical Heat Flux During the Cooling of Power Electronics. International Refrigeration and Air Conditioning Conference, Purdue, USA.
- IEEE Standards Association. (2018). *IEEE Recommended Practice for 1 kV to 35 kV Medium-Voltage DC Power Systems on Ships*. IEEE Std 1709™-2018. New York, USA.
- Infineon Technologies AG. (2018). *FZ1200R45KL3\_B5*. Munic, Germany. (datasheet).
- Islam, M. D., Mahfuz-Ur-Rahman, A. M., Muttaqi, K. M., & Sutanto, D. (March 2019). State-of-the-Art of the Medium-Voltage Power Converter Technologies for Grid Integration of Solar Photovoltaic Power Plants. *IEEE Transactions on Energy Conversion*, 34(1), S. 372-384.
- Lemmon, E. W., Bell, I. H., Huber, M. L., & McLinden, M. O. (2018). NIST Standard Reference Database 23: Reference Fluid Thermodynamic and Transport Properties - REFPROP, Version 10.0., *National Institute of Standards and Technology, Standard Reference Data Program*. Gaithersburg.
- Siemens AG. (2021). *Large Drive Applications : Motors for every demand*. Nuremberg, Germany.
- Siemens Energy. (2021). *MVDC PLUS : Medium Voltage Direct Current Managing the future grid*. Erlangen, Germany. (white paper).

## ACKNOWLEDGEMENT

The authors acknowledge the financial support provided by die *Sächsische Aufbaubank – Förderbank – (SAB)*.